# The Pan-STARRS1 Photometric System

J.L. Tonry,[1] C.W. Stubbs,[2,3] K.R. Lykke,[4] P. Doherty,[3] I.S. Shivvers, [2,5] W.S. Burgett,[1]
K.C. Chambers,[1] K.W. Hodapp,[1] N. Kaiser,[1] R.-P. Kudritzki,[1] E.A. Magnier,[1]
J.S. Morgan,[1] P.A. Price,[7] and R.J. Wainscoat [1]

## ABSTRACT

The Pan-STARRS1 survey is collecting multi-epoch, multi-color observations of the sky north of declination $-30°$ to unprecedented depths. These data are being photometrically and astrometrically calibrated and will serve as a reference for many other purposes. In this paper we present our determination of the Pan-STARRS1 photometric system: $g_{P1}$, $r_{P1}$, $i_{P1}$, $z_{P1}$, $y_{P1}$, and $w_{P1}$. The Pan-STARRS1 photometric system is fundamentally based on the HST Calspec spectrophotometric observations, which in turn are fundamentally based on models of white dwarf atmospheres. We define the Pan-STARRS1 magnitude system, and describe in detail our measurement of the system passbands, including both the instrumental sensitivity and atmospheric transmission functions. Byproducts, including transformations to other photometric systems, galactic extinction, and stellar locus are also provided. We close with a discussion of remaining systematic errors.

*Subject headings:* instrumentation: photometers — techniques: photometric — atmospheric effects — Surveys:

[1]Institute for Astronomy, University of Hawaii, 2680 Woodlawn Drive, Honolulu HI 96822

[2]Harvard-Smithsonian Center for Astrophysics, 60 Garden Street, Cambridge, MA 02138

[3]Department of Physics, Harvard University, 17 Oxford Street, Cambridge MA 02138

[4]National Institute of Standards and Technology, 100 Bureau Drive, Gaithersburg MD 20899, USA

[5]Department of Astronomy, University of California, Berkeley CA 94720

[6]Department of Physics and Astronomy, Johns Hopkins University, 3400 North Charles Street, Baltimore, MD 21218, USA

[7]Department of Astrophysical Sciences, Princeton University, Princeton, NJ 08544, USA

[8]US Naval Observatory, Flagstaff Station, Flagstaff, AZ 86001, USA

# 1. INTRODUCTION

## 1.1. Photometry and Astronomy

All ground-based photometry measures light that has been filtered by passage through the atmosphere and by an optical system that typically includes a bandpass filter. The surviving light is finally converted into an electrical signal by a detector. The system therefore presents a net capture cross section, $A(\nu, \theta, t)$, to incoming photons that depends on frequency $\nu$ (or wavelength), direction $\theta$ with respect to the boresight (or detector pixel), and time, where "capture cross section" quantifies the probability of counting an incident photon as an $e^-$ in the detector.

An object with a spectral energy distribution (SED) $f_\nu$ [erg/s/cm$^2$/Hz] whose light arrives at the top of the atmosphere therefore creates a signal of $\int f_\nu (h\nu)^{-1} A(\nu, \theta, t) \, d\nu$ in a photon-sensitive detector. If the instrument's bandpass encompasses significant wavelength variation in $A(\nu, \theta, t)$ or $f_\nu$ it is *not* possible to recover $f_\nu$ uniquely from an observation: information is necessarily lost, and different SEDs can produce the same signal. In many cases we are interested in a restricted question, however; we believe we know the spectral form of the SED of an object, but we do not know the overall normalization. In this case we can recover this normalization by simply integrating a unity-normalized SED against the known cross section $A(\nu, \theta, t)$, and then scale to the true SED by the ratio of the observed signal to this integral.

Astronomical magnitude systems are based on this concept, as summarized by Bessell (2005). The "Vega normalized" system, developed when instrumentation was capable of much higher relative accuracy than absolute, uses A0 stars (e.g. Vega) as the reference. That is, a "Vega magnitude" is the ratio of the signal produced by integrating an object's SED through $A(\nu, \theta, t)$ compared to the A0 star Vega, where "A0 star" has evolved to a loosely defined set of stars whose SEDs are believed to be known at the few percent level, and whose cataloged magnitudes are fairly self consistent with the SEDs. (In retrospect, the choice of bright A0 stars with enormous H absorption for the standard SED was less than optimal.) This magnitude system is therefore operationally defined from a catalog as opposed to physically defined, and systematic inaccuracies accrue from the definition as well as from uncertain knowledge of bandpasses and detector sensitivities.

Another magnitude system, heartily endorsed by Pan-STARRS1, is the "AB system" (Oke & Gunn 1983), described in detail for the Sloan Digital Sky Survey (SDSS, York et al. (2000)) by Fukugita et al. (1996). In this system a "monochromatic AB magnitude" is just

a logarithm of flux density:

$$m_{AB}(\nu) = -2.5 \log(f_\nu/3631 \text{ Jy}) \tag{1}$$
$$= -48.600 - 2.5 \log(f_\nu[\text{erg/sec/cm}^2/\text{Hz}]) \tag{2}$$
$$= 16.847 - 2.5 \log(f_\gamma[\text{ph/sec/cm}^2/\text{dln } \lambda]). \tag{3}$$

where $1 \text{ Jy} = 10^{-23} \text{erg/sec/cm}^2/\text{Hz}$, $f_\gamma$ only differs from $f_\nu$ by a factor of $h$ but is integrated against $\text{dln } \lambda = d \ln \nu$ without needing a factor of $(h\nu)^{-1}$, and the constant was chosen to set the AB mag of Vega at 548 nm to be 0.03, the $V$ mag of Vega, under the assumptions that the "effective wavelength" of the V band for Vega was 548 nm. A "bandpass AB magnitude" is defined similarly:

$$m_{AB} = -2.5 \log \left( \frac{\int f_\nu \, (h\nu)^{-1} \, A(\nu) \, d\nu}{\int 3631 \text{ Jy} \, (h\nu)^{-1} \, A(\nu) \, d\nu} \right). \tag{4}$$

There is no arbitrariness in the magnitude definition for a given well-defined capture cross section $A(\nu)$[1].

In practice we do not burden every flux observation with a detailed $A(\nu, \theta, t)$, so we instead alter the flux we report to reflect the flux we think it would have had if subjected to a nominal $A(\nu)$ instead of the actual, momentary $A(\nu, \theta, t)$. This correction has a number of components, including removing the dependence on $\theta$ by correcting for detector response, optics vignetting and other spatial variations, and most significantly, adjusting the flux for the instantaneous "atmospheric extinction". The $\nu$-independent component of this amounts merely to a renormalization of sensitivity; the $\nu$-dependent component creates a new source of error that depends on the particular SED being observed, generally quantified as a "color term", a correction for stellar SEDs consisting of a coefficient that multiplies a color.

Because of the ambiguity when inferring an AB magnitude from a flux measurement when the SED is not known, there is a choice to be made between trying to report an AB magnitude that is "universal" (e.g. what would be observed without any atmospheric extinction) versus what is actually observed. The tradition of "regression to top of atmosphere" makes sense for a limited set of SEDs such as stars, but non-stellar SEDs (e.g. very cool stars, AGN at high redshift, supernovae, etc.) are becoming so important, that Pan-STARRS1 has

---

[1]The classic observer's "magnitude" system, originally defined by Pogson to crudely coincide with ancient Greek classification of star brightness, is slowly withering in favor of flux densities reported in units of Jy, but we caution that such flux densities typically *are* ambiguous for extended bandpasses, and we *strongly* recommend that non-monochromatic "flux densities" conform to this definition of the AB system: A non-monochromatic "flux density" is the ratio of detector response to SED relative to constant $f_\nu$.

adopted the approach of modern photometric systems such as SDSS: bandpasses explicitly include a nominal level of atmospheric extinction.[2]

The actual determination and implementation of the $AB$ magnitude system for Pan-STARRS1 can be carried out in different ways. One option is to infer AB magnitudes through synthetically derived bandpasses by various methods such as 1) exploiting the overlap between Pan-STARRS1 and another extensive catalog of stellar magnitudes such as SDSS, 2) using the stellar locus in color-color space (subject to removal of dust reddening), or 3) observing spectrophotometric standard stars and regressing out atmospheric extinction. In effect this transfers an extant $AB$ calibration (for better or for worse) to Pan-STARRS1 photometry.

Another option (described in Stubbs & Tonry (2006)) is to obtain independent determinations of the instrumental and atmospheric response functions, establishing the wavelength-dependent part of $A(\nu)$. In principle it is possible to determine the absolute sensitivity of the Pan-STARRS1 system, but in practice we can also depend on spectrophotometric standard star observations to verify the bandpasses and set the overall normalization.

Once a set of stars are provided with accurate AB magnitudes, the system can be propagated around the sky using overlapping observations to disentangle instrumental and atmospheric contributions. This was used successfully by Padmanabhan et al. (2008) for the SDSS survey and is currently being implemented for Pan-STARRS1 by Schlafly & Finkbeiner (2012).

The consistency of these different techniques can be used to assess systematic errors in the survey's photometric calibration, but we defer a detailed comparison of these different approaches to a subsequent paper. Our initial comparisons indicate that the Pan-STARRS1 implementation of the $AB$ system has an accuracy of $\sim 0.02$ mag (90% confidence), where the dominant contribution is uncertainty in how well spectrophotometry matches the AB system.

For this paper we use a combination of measurements of our instrumental and atmospheric response function with spectrophotometric star observations to establish the Pan-STARRS1 photometric system. The Pan-STARRS1 calibration described here is fundamentally based upon the Calspec spectrophotometric standards from Hubble Space Telescope (HST) (Bohlin *et al.* 2001).

---

[2]Pan-STARRS1 does *not*, however, adhere to the SDSS practice of reporting inverse hyperbolic sines (luptitudes) in place of magnitudes; this practice arose from attempting to serve two priors (object power, for which a logarithm is appropriate, versus net observed flux, for which linear is better) with one number. The Pan-STARRS1 databases simply serve up both flux and magnitude.

## 1.2. Pan-STARRS1

The Pan-STARRS1 system is a 1.8 m aperture, f/4.4 telescope (Hodapp *et al.* 2004) illuminating a 1.4 Gpixel detector spanning a 3.3° field of view (Tonry *et al.* (2008) and Onaka *et al.* (2008)), located on Haleakala (Kaiser et al. (2010)), and dedicated to sky survey observations (Chambers *et al.* (in prep)). The Pan-STARRS1 filters are designated $g_{P1}$, $r_{P1}$, $i_{P1}$, $z_{P1}$, $y_{P1}$, and $w_{P1}$ in order to clearly distinguish PS1 from other photometric systems. The gigapixel camera (GPC1) consists of an $8 \times 8$ array of orthogonal transfer array (OTA) CCDs, and each OTA is subdivided into an $8 \times 8$ array of "cells", each an independent $590 \times 598$ $10\mu m$ pixel CCD. Images obtained by the Pan-STARRS1 system are processed through the Image Processing Pipeline (IPP) (Magnier 2006). Although the filter system for Pan-STARRS1 has much in common with that used in previous surveys such as SDSS (York et al. 2000), the $g_{P1}$ filter extends 20 nm redward of $g_{SDSS}$, paying the price of 5577Å sky emission for greater sensitivity and lower systematics for photometric redshifts, the $z_{P1}$ filter is cut off at 920 nm, giving it a different response than the detector response defined $z_{SDSS}$, and SDSS has no corresponding $y_{P1}$ filter.

AB magnitudes reported by Pan-STARRS1 include an explicit model for the atmospheric extinction at a nominal airmass (1.2), with relatively small corrections applied to the observed fluxes to bring them to this airmass. Given a known SED that differs from $f_\nu$=const, it is therefore possible to convert the "top of atmosphere" magnitude reported by Pan-STARRS1 back to the nominal airmass, and from that correct for the atmospheric extinction for the particular SED. This correction may be small or parameterizable by "color terms" if the SED is similar to that of a star, but it can be very significant for an object with an emission line in an atmospheric absorption band.

As described at length by Stubbs & Tonry (2006), Stubbs et al. (2007), and Stubbs et al. (2010) we believe that it is possible, at least in principle, to calibrate the Pan-STARRS1 system as an precise photometer, permitting measurement of absolute fluxes with no reliance on standard stars whatsoever. Although we currently fall distinctly short of this ideal, the next section describes our progress in implementing such a calibration.

The third section presents the Pan-STARRS1 system: Pan-STARRS1 bandpasses, derived quantities such as conversions to other bandpasses, Galactic extinction in the Pan-STARRS1 bandpasses, the stellar locus in Pan-STARRS1 bandpasses, and color terms from filter non-uniformities and detector differences.

The penultimate section discusses sources of systematic error such as uncertainties in bandpasses, imperfect knowledge of the atmosphere, and uncertainties in flux determination. We also describe some of the foundational systematic errors such the accuracy with which

SEDs do match the AB system and point out inconsistencies between the Pan-STARRS1 and SDSS photometric systems.

We conclude with an assessment of the present state of photometric accuracy, the Pan-STARRS1 strategy for carpeting the sky with photometry accurate to better than 1 percent, and the next steps towards our goal of photometry based on NIST calibrated equipment rather than standard stars.

## 2.  PHOTOMETRIC CALIBRATION OF Pan-STARRS1

We factor the Pan-STARRS1 system's cross section $A(\nu, \theta, t)$ into three terms: the "throughput" of the optics and detector combination (common to observations made in all filters), the filter bandpasses, and the atmosphere. Each of these terms presents unique challenges for measurement and for monitoring since they change on different timescales.

We have measured each of these factors, and in our judgement the best information we have comes from

- Throughput, including transmission of optics and QE of detector: obtained by a comparison against a calibrated photodiode as a function of wavelength, normalized and tweaked by 3% RMS into agreement with spectrophotometric standard stars.

- Transmission of filters: manufacturer's measurements verified by in-situ measurement, tweaked by 1% RMS into agreement with spectrophotometric standard stars.

- Atmospheric transmission: MODTRAN models, aerosol extinction tweaked into agreement with nightly regression against airmass.

This approach exploits external information for those aspects of $A(\nu)$ that have rapid spectral variation (filter edges and atmospheric absorption lines), while using the standard star observations to establish the overall normalization across the different filter bands, by applying a low order "tweak" to $A(\nu)$ to achieve agreement between synthetic and observed photometry.

This section presents a brief synopsis of the measurement of the instrumental and atmospheric response factors, and the details the procedure we used for bringing them into agreement with Calspec spectrophotometry.

## 2.1. Instrumental Transmission

We have previously described (Stubbs et al. 2010) an in-dome determination of the Pan-STARRS1 filters and instrumental sensitivity function, but we undertook new measurements that avoid the unwanted contributions from scattered light and from ghosting in the optical system. We used an Ekspla laser that can be tuned from 400 nm to 1100 nm, wavelength calibration checked against an emission line source using a spectrometer. The laser light was transmitted by a fiber into a 75 mm projection telescope that created a spotlight beam we fed into the Pan-STARRS1 optics. A NIST-calibrated photodiode was placed directly in the projection telescope beam in order to measure the relative photon flux as a function of wavelength; no attempt was made to measure the absolute flux or collecting area of Pan-STARRS1.

The beam from the projection telescope was placed near the mean radius of the Pan-STARRS1 pupil, angled down the boresight to avoid all scatterers and arrive at the center of GPC1, and defocused slightly to create spots of diameter 1.0° or 1.7° that span many OTAs. The basic exposure comprises opening the GPC1 shutter, opening the laser shutter and integrating the total light received by the photodiode, closing the laser shutter when a predetermined level has been received, and then closing the GPC1 shutter. Observations of this sort are interleaved with "dark" exposures of identical duration but without any laser light, and the "dark" levels are subtracted from both the signal from GPC1 and the photodiode. The resulting images were then "flatfielded" by dividing by the gain for each cell's amplifier, creating images whose values are the $e^-$ created in each cell. (GPC1 includes a deployable $^{55}$Fe source inside the cryostat; a $K\alpha$ xray photon converts to 1620 electrons in silicon; analysis of these events provides the conversion between $e^-$ to ADU.)

Many sets of observations were collected between 400 nm and 1100 nm in 2 nm steps through each filter and with no filter. Normalized by the photodiode, the ratio of filter to no filter immediately provided a measure of filter throughput, albeit in nearly parallel light at a fairly representative angle off of normal. The normalized fluxes with no filter in the beam give us the optics and detector throughput, once they are corrected for ghosts and scattering of IR light within the silicon, both of which remove light from a small PSF but leave it within the projected spot.

The Pan-STARRS1 optical system has a particularly important ghost that is created by light bouncing off of the CCD, the back surface of the first corrector lens, and then being nearly refocussed onto the detector again. We exploited the shadow of the photodiode in the projected spot to evaluate the ghost amplitude as well as observations where the projected spot was focussed to 0.3° and put off center. We found the ghost amplitude to be somewhat larger than expected from the manufacturer's estimates of reflectivities of CCD

and AR coating on the lens, particularly at the very blue and red ends of the spectrum. We speculate that this arises because of one or more imperfect or degraded lens AR coatings, and this is the reason that the in-situ measurement of throughput is so important.

At wavelengths approaching the bandgap Si becomes more and more transparent, so some fraction of light passes fully through the collecting volume, and is absorbed after one or more reflections. This signal is accumulated over a very large (mm scale) skirt, but does not contribute usefully to the signal to noise of a tiny PSF and therefore should not be included as part of the system throughput. Tonry $et$ $al.$ (1997) discusses of how this effect was important in the $I$ band for the SBF survey; it was also the reason that SDSS elected to use thick CCDs for the $z$ band (Gunn et al. 1998). For the 75 $\mu$m thick Pan-STARRS1 detectors it becomes important in the $y_{P1}$ filter, and we have applied a semi-empirical correction to the Pan-STARRS1 throughput curve to account for it.

The QE of silicon depends on detector temperature at very red wavelengths, and we also took the opportunity to measure the detector sensitivity as a function of temperature between 140 K and 190 K, from which we constructed temperature coefficients for the $y_{P1}$ filter. (At 1 $\mu$m we find the relative QE changes by about $+0.3\%$/K at 190 K.)

For comparison with the in-situ throughput measurement we assembled manufacturer's measurements of reflectivities of the primary and secondary mirrors, the transmission of the three corrector lens AR coatings, and the QE measurements performed in the lab for each of the CCDs scaled to a common temperature of 193 K.

Figure 1 illustrates the good agreement between the in-situ measurements and the product of these lab throughputs. We have no absolute transmission normalization from our in-situ measurements, so its absolute level is set by comparison with standard stars. The "tweak" that we use to bring the in-situ, laser measurements into agreement with photometric standards is described below. Multiplying the lab throughputs by the Pan-STARRS1 aperture of 1.8 m and mean geometrical transmission past secondary and baffles of 0.62, we found that we could match the flux detected from standard stars if we incorporated an additional factor of $\sim 0.9$, very plausibly the result of absorption or scattering by dust and degradation.

The spot sizes of the in-situ measurements were chosen to have small variation in vignetting and therefore require negligible flatfield correction. For on-sky observations, the IPP corrects for small-scale spatial non-uniformities by dividing by images off of the flatfield screen. Large-scale non-uniformities are corrected using observations of stars dithered widely across the field of view during times of constant atmospheric extinction. We thus reduce $A(\nu, \theta, t)$ to $A(\nu, t)$, at least for an SED that is approximately that of a late K star. We
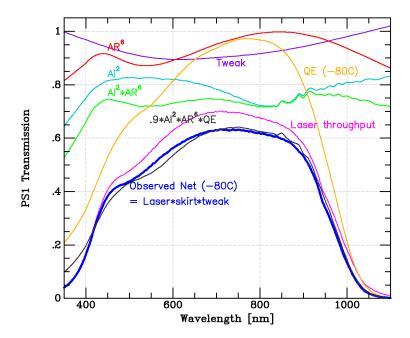
Fig. 1.— The various components of the relative throughput (detected electrons per incident photon) of the Pan-STARRS1 optical system and detector are shown. The heavy blue line, "Laser throughput" times the "Tweak" times a correction for IR skirt, is our best estimate of the Pan-STARRS1 throughput. The adjacent gray line, $0.9 \times \mathrm{Al}^2\mathrm{AR}^6\mathrm{QE}$, is an alternative estimate. The differences we believe are the result of AR coating degradation. Values below 400nm are extrapolations, but no Pan-STARRS1 filter has a significant response there.

detail below color terms for other SEDs.

## 2.2. Filter Transmission

The Pan-STARRS1 filters, interference coatings on 1 cm of fused silica manufactured by Barr Precision Optics (now Materion), are located 0.4 m above the focal plane. Barr provided transmission measurements using an f/8 beam at 10 radii ranging from 1 to 9.5 inches and 8 azimuths at the 9.5 inch radius. Some of the filters have substantial variation in transmission as a function of radius, although they appear to have a high degree of azimuthal symmetry. Although the pupil is a ∼100 mm diameter donut on the filters, color differences arise as a function of position.

The f/4.4 Pan-STARRS1 beam is incident on the filters at angles up to 6.5° off of normal, with a pupil-averaged angle of 5.4°. This leads to a shift in transmission to the blue in the Pan-STARRS1 beam relative to Barr's nearly parallel-light data by $(1 - \sin^2\theta/n^2)^{1/2}$. Calculations of Barr filter transmission at 0.0° and 9.9° off of normal provided an accurate coefficient for the wavelength shift of 0.48% at an angle of incidence of 9.9°. For each of the six filters and 12 field positions we ray-traced 10,000 positions across the PS1 pupil, and added up the Barr traces with appropriate wavelength shift as a function of incident angle. We finally summed up a grand average that is the area-weighted transmission out to field angles of 1.5°. This is illustrated in Figure 2.

Our in-situ measurements of the Barr filters confirmed the accuracy of the Barr traces of the filters. The overall transmission and filter edges as well as the spectral bumps and wiggles are matched to a very satisfactory degree. As with the throughput measurement, however, we describe below percent-level tweaks that we require to match standard star observations.

## 2.3. Atmospheric Transmission

The third component of the Pan-STARRS1 photometric system is the atmosphere. As described in Stubbs et al. (2007), Burke et al. (2010), and Patat *et al.* (2011), atmospheric attenuation per airmass $k$ is a sum of Rayleigh scattering from interactions with atmospheric components small compared to the wavelength ($k \sim \lambda^{-4}$), Mie scattering off aerosols of comparable size ($k \sim \lambda^{-1.4}$), cloud scattering from large water and ice particles ($k \sim \text{const}$) and molecular absorption. Rayleigh scattering and molecular absorption normally depend only on the integrated density along the line of sight and are temporally stable for stable
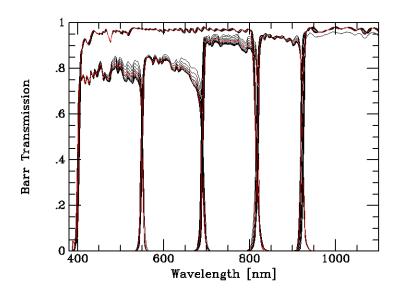
Fig. 2.— Filter transmission of the six Pan-STARRS1 filters. $g_{P1}$, $r_{P1}$, $i_{P1}$, $z_{P1}$, $y_{P1}$, and $w_{P1}$ are shown as a function of field angle, in 0.15° steps to 1.65°, and the red curve shows the area weighted average. Small field angles tend to have similar transmissions, allowing their curves to be distinguished from large field angle.

molecule concentrations (e.g. $O_2$ but not $H_2O$). Cloud scattering obviously is extremely variable, particularly over the large field of view of Pan-STARRS1. Aerosols arise from volcanic eruptions, smoke, and dust and are highly variable, both in amplitude as well as spectral shape, and the $-1.4$ power law is very approximate. Patat *et al.* (2011) make the point that volcanic events should not be thought of as creating brief increases in aerosol extinction, but instead, times of low and constant aerosol extinction are exceptionally rare.

In order to manage the complexity of different atmospheric extinction components as well as to provide the high spectral resolution that can be important for non-stellar SEDs, we use the MODTRAN program (Anderson *et al.* 2001) to compute atmospheric transmission to the peak of Halekala for a range of zenith angles and water vapor content. The MODTRAN "Generic Tropical" model atmosphere was used, with "Desert Extinction (Spring-Summer)" aerosol choice. No attenuation from clouds was included. An alternative atmospheric model from Atmospheric and Environmental Research[3] has been used by Patat *et al.* (2011) and we are confident that it would be equally satisfactory.

For each Pan-STARRS1 bandpass we integrated a set of power law SEDs against each of these model atmospheres and created an interpolation function for the extinction as a function of four variables: $z$ for airmass ($\sec\zeta$ where $\zeta$ is the zenith angle), $h$ for precipitable water vapor (PWV) (typically $0.65\,\mathrm{cm}$ at sea level), $a$ for "aerosol exponent" (nominally 1; we modify the Modtran aerosol component by applying this power to the aerosol transmission, thereby mostly affecting the aerosol amplitude), and $p$ for SED power law. ($p = +2$ for $f_\nu \sim \nu^{+2}$ corresponds to an O star with $(r-i) = -0.43$, $p = 0$ for $f_\nu \sim$ const corresponds to an F star with $(r-i) = 0.00$, and $p = -2$ for $f_\nu \sim \nu^{-2}$ corresponds to an K5 star with $(r-i) = +0.42$. Note that $(g-r) \sim 0.2 + 1.9(r-i)$ in this range.) The extinction $dm$ in magnitudes is given by

$$\ln dm = \ln C + Z \ln z + A \ln a + Pp + \ln h(H_0 + H_1 \ln z + H_2 \ln h) \qquad (5)$$

The coefficients for each of the Pan-STARRS1 filters are given in Table 1.

The interpolation Formula 5 offers only limited adjustability in the extinction coefficients via the aerosol transmission exponent $a$, essentially adjusting the aerosol amplitude but not its spectral shape. Therefore matching observations of standards as a function of airmass on a given night may call for additional term $\delta k \sec\zeta$. In addition, ozone absorption in the $r_{\mathrm{P1}}$ band is significant, and $O_3$ does vary somewhat (Patat *et al.* (2011) find a peak-to-peak yearly variation of 0.01 mag in $k_r$). The total column of $O_3$ is usually expressed in "Dobson units" (DU, $10\,\mu\mathrm{m}$ thick layer at STP), and we find the effect of $DU$ ozone column on the

---

[3]http://rtweb.aer.com

Table 1: Pan-STARRS1 Extinction Coefficients

| Filter | $C$ | $Z$ | $A$ | $P$ | $H_0$ | $H_1$ | $H_2$ | err |
|--------|-----|-----|-----|-----|-------|-------|-------|-----|
| $g_{P1}$ | 0.204 | 0.982 | 0.227 | 0.021 | 0.001 | −0.000 | 0.000 | 1.7 |
| $r_{P1}$ | 0.123 | 0.975 | 0.283 | 0.012 | 0.012 | −0.000 | 0.005 | 2.0 |
| $i_{P1}$ | 0.092 | 0.831 | 0.304 | 0.005 | 0.125 | −0.011 | 0.035 | 2.7 |
| $z_{P1}$ | 0.060 | 0.878 | 0.375 | −0.004 | 0.330 | −0.070 | 0.055 | 4.9 |
| $y_{P1}$ | 0.154 | 0.680 | 0.145 | 0.014 | 0.549 | −0.084 | 0.024 | 3.5 |
| $w_{P1}$ | 0.139 | 0.936 | 0.259 | 0.075 | 0.029 | −0.002 | 0.009 | 2.2 |
| $Open$ | 0.137 | 0.897 | 0.244 | 0.112 | 0.093 | −0.018 | 0.020 | 4.6 |

Note. — The columns contain coefficients described above for that interpolate the Modtran extinction calculations each of the Pan-STARRS1 bandpasses. The final column is the percentage scatter of these fits relative to the calculated values. Note that the saturation of molecular lines means that the extinction is *not* proportional to $\sec \zeta$ ($Z \neq 1$), particularly $y_{P1}$.

$r_{P1}$ extinction coefficient to be $\delta k_r = 1.0 \times 10^{-4}(DU - 260)$. (Ozone column can be obtained from OMI/TOMS satellite measurements[4].)

In order to monitor the water content $h$ of the atmosphere, we deployed a 180 mm astrograph (the "spectroscopic sky probe") with a coarse diffraction grating across the aperture, and pointed it at the north celestial pole (Shivvers et al. in prep). It has been in continuous operation since June 2011. The spectrum of Polaris provides equivalent widths of water bands, the most important at 723 nm, 822 nm, and 946 nm, as well as the A and B bands of $O_2$.

We found that the atmospheric absorption was accurately matched by the MODTRAN models, and that we could infer a value for $h$ that is accurate to about 10% from the observed equivalent widths. For example, MODTRAN models produce an equivalent width for the water band between 810–836 nm of EW = 0.79 nm $h^{0.74}$ $\sec^{0.75} \zeta$, and comparison with the Polaris observations allows us to determine $h$. The mean PWV $h$ of 0.65 cm varies by about 50% RMS over long periods, although it tends to be much more stable than that during a night. We therefore have adopted PWV of 0.65 cm as the water column for the nominal Pan-STARRS1 bandpasses; it affects $i_{P1}$, $z_{P1}$, $w_{P1}$, and especially $y_{P1}$.

[4]http://oozoneaq.gsfc.nasa.gov

## 2.4. Synthetic Photometry

We collected the SEDs of 783 spectrophotometric standards, including 59 STIS Calspec photometric standards (Bohlin *et al.* 2001), which range from the Sun to Vega to stars fainter than $V = 15$ mag[5]. The fundamental basis for this photometry derives from models of hydrogen white dwarf atmospheres (Bohlin 2007) and comparisons between Vega and blackbodies, summarized by Hayes & Latham (1975) and Hayes (1985). The spectrophotometry of Gunn and Stryker (Gunn & Stryker 1983), augmented by Bruzual and Persson to include the UV and IR provided another 175 SEDs[6] There are 379 relatively bright stars from the "Next Generation Spectral Library" from STScI, although caution is indicated for stars with poor slit centering[7]. The 4 SDSS spectrophotometric standards from Fukugita et al. (1996) were included as well as their spectrum of Vega. The Pickles spectrophotometry library includes 131 stellar SEDs spanning a range of temperature and luminosity (Pickles 2011)[8]. Finally we included 23 spectrophotometric observations of very cool stars from the SPEX prism database as well as 11 optical spectra of brown dwarfs from Mike Cushing (private communication)[9].

We also assembled Johnson $B$ and $V$ and Cousins $R$ and $I$ bandpasses from Bessell (1990) (noting their convention of "energy sensitivity functions" that have units of photons per erg and Vega normalization). The $J$, $H$, and $K_s$ IR bandpasses and zeropoints ("energy sensitivity" and Vega normalized) of the 2MASS survey were obtained from Cohen et al. (2003) and the 2MASS website[10] since 2MASS provides a full-sky homogeneous set of observations. Note that other definitions of $JHK_s$ such as the "MKO-NIR" set described by Simons & Tokunaga (2002) or the UKIDSS survey differ somewhat. The SDSS bandpasses are presented in Fukugita et al. (1996), but were derived from the recommendations on the SDSS website[11].

Finally, we have Pan-STARRS1 bandpasses that are the product of atmosphere, optics and detector throughput, and filter.

---

[5]http://www.stsci.edu/hst/observatory/cdbs/calspec.html

[6]http://ftp.stsci.edu/cdbs/grid/bpgs

[7]http://archive.stsci.edu/prepds/stisngsl

[8]http://cdsarc.u-strasbg.fr/viz-bin/ftp-index?J/PASP/110/863

[9]http://web.mit.edu/ajb/www/browndwarfs/spexprism/index.html

[10]http://www.ipac.caltech.edu/2mass/releases/allsky/doc/sec6_4a.html

[11]http://www.sdss.org/dr3/instruments/imager/#filters

We multiply all of these SEDs by each bandpass and integrate to obtain predictions for flux, magnitude, and color (either AB or Vega depending on the bandpass). Our calculation keeps careful track of uncertainties in the SED and tries to estimate uncertainty when an SED and a filter do not completely overlap.

## 2.5. Standard Star Observations

MJD 55744 (UT 02 July 2011) was a photometric night during which we observed a substantial number of spectrophotometric standard stars from the STIS Calspec (Bohlin *et al.* 2001) tabulation: 1740346, KF01T5, KF06T2, KF08T3, LDS749B, P177D, and WD1657-343. These were observed throughout the night at airmasses between 1 and 2.2 in all six filters and also with no filter in the beam. Each observation was repeated, and exposure times were chosen to stay well clear of any non-linearities but still permit good accuracy. In addition, Medium Deep Field 9 (MD09), which overlaps SDSS Stripe82, was observed a dozen times in each of $g_{P1}$, $r_{P1}$, $i_{P1}$, $z_{P1}$, and $y_{P1}$, providing the opportunity to tie the spectrophotometric data to a well-observed Pan-STARRS1 field. All standard stars were placed on OTA 34 and cell 33, so their integration was on the same silicon and used the same amplifier for read-out (gain measured to be 0.97 e$^-$/ADU).

The observations were bias subtracted and flatfielded as part of the normal IPP processing, and the IPP fluxes (instrumental magnitudes) were then available for comparison with tabulated SEDs. The IPP performs an aperture correction and reports fluxes within a radius of 25 pixels (13″ diameter).

Observations of Polaris on MJD 55744 with the spectroscopic sky probe had a PWV indistinguishable from the long term mean of 0.65 cm.

## 2.6. Photometry Refinement

The Pan-STARRS1 cross section $A(\nu, t)$ for capturing photons is obtained by multiplying the factors of atmosphere for a given observation, the in-situ measurements of optics and detector throughput, and the filter transmission. In principle there are only two unknown parameters: a single overall normalization factor, required because the in-situ throughput measurements did not attempt to evaluate the net collecting area of the telescope, and the aerosol extinction exponent $a$ for the night of the standard star observations.

In practice, we found that small "tweaks" were required to bring observations into agreement with spectrophotometry. The need for these tweaks is not surprising because

our measurement technique currently has the potential for systematic error at the several percent level (for example, we sample the telescope pupil at only one point, ghost image and scattered light compensation, chromatic effects from fiber in illumination of photodiode, etc), and we are trying to achieve 1% accuracy. However, the excellent agreement between the laser and Barr measurements of the filter band edges and transmission wiggles led us to parameterize the tweaks as a smooth adjustment to the throughput function and individual transmission adjustments for each filter[12]. There is an ambiguity between whether tweaks should be applied to throughput or filter, and we have attempted to disentangle them as best we can using the information from overlapping bandpasses ($w_{P1}$ overlaps $g_{P1}$, $r_{P1}$, and $i_{P1}$) and standard star observations with no filter.

We adjust a total of 12 parameters for the Pan-STARRS1 system: 9 parameters provide offset and spectral tilt tweaks for throughput and each filter (expected to be durable at the 1% level for very long periods), 2 parameters characterize the aerosol extinction (changes nightly), and 1 parameter sets the overall collecting area (expected to slowly change with dust and degradation of optical surfaces).

The Pan-STARRS1 no-filter cross-section $A_0(\nu)$ consists of the area of a 1.8 m disk, times the geometrical loss from secondary and baffles of 0.62 derived from ray tracing, times in-situ throughput measurements, adjusted for IR light scattering in the Si and normalized to a peak of 0.70 (the peak of the product of Al reflectivities, AR coatings, and CCD QE), times the tweak function. The tweak function we adopted consists of a natural spline with five knots at 400, 550, 700, 850, and 1000 nm and values we determined to be 0.035, 0.113, 0.113, 0.081, and 0.022 mag (positive meaning less sensitive). The mean across the optical of 0.085 mag simply measures the wavelength-independent deviation from the arbitrary 0.70 peak throughput and amounts to a normalization correction. The spectral variation of 0.030 mag RMS is the mis-match between our in-situ instrumental throughput measurements and the spectrophotometric standard observations, after making the aerosol adjustment to the atmospheric transmission. This tweak function is illustrated in Fig 1.

The filter-specific tweaks were determined to be 0.012, 0.019, 0.009, −0.009, −0.010, −0.005 mag for $g_{P1}$, $r_{P1}$, $i_{P1}$, $z_{P1}$, $y_{P1}$, and $w_{P1}$ (positive is less sensitive; the mean of $i_{P1}$ and $z_{P1}$ is constrained to zero).

The procedure for determining these parameters involves iterating a comparison between

---

[12]We emphasize that we are *not* attempting to determine zeropoints for each filter individually; we determine *one* zeropoint for the Pan-STARRS1 system and these transmission offsets and throughput tweaks represent the extent to which we were unsuccessful (3%) in our in-situ measurements (or conceivably error in the spectrophotometric standard SEDs).

synthetic photometry using spectrophotometric SEDs with observations of standard stars and stellar locus. The combination of our atmospheric transmission model and the system transmission measurements produce (untweaked) synthetic photometry that disagrees with the observations by 0.1 mag peak-to-peak from $g_{P1}$ to $y_{P1}$. We have elected to trust the Calspec SEDs as the foundational calibration data, and we adjust the response functions to achieve photometric consistency.

For each of the seven Calspec spectrophotometric standards observed on MJD 55744 we calculated predictions for the flux (including color terms appropriate for the actual filter location and OTA on which they were observed), and adjusted the parameters to match the observations. We found that the variation with airmass called for modification of the MODTRAN extinction with an aerosol exponent $a = 0.7$ and an additional $\delta k = -0.02$ mag/airmass (i.e. aerosols were lighter than the MODTRAN default by about 30% and had a steeper rise at bluer wavelengths). The standards had a large enough diversity in color ($-0.38 < (r - i) < +0.35$) to provide some constraint on the filter tilt parameters (spline knots).

As another check, we computed a "stellar locus" from all of the spectrophotometric standards. This involves de-reddening the SEDs of galactic extinction, computing synthetic colors in the Pan-STARRS1 bandpasses, and fitting various colors as a function of $(r-i)_{P1}$. Uncertainties in Galactic extinction were propagated into the colors. Each of the standard star observations and MD09 includes thousands of stars over the field of view, and these magnitudes were de-reddened as well using Schlegel et al. (1998) (SFD) values for Galactic extinction. The comparison provides us with a second constraint on the tweak parameters, and is the reason that the mean offsets of the standard star observations are not simply zero. The huge color range of field stars creates the strongest constraint on the filter tilt parameters. Figure 3 shows the observed stellar colors with the spline curves from the spectrophotometric standards overplotted.

We also calculated Pan-STARRS1-SDSS color transformations, computed Pan-STARRS1 magnitudes from SDSS magnitudes in Stripe82 obtained from Zeljko Ivezic[13], and compared them to the observed magnitudes of stars in the MD09 observations on MJD 55744. This was *not* used to adjust parameters, however. Table 2 shows the difference between the fluxes observed for the spectrophotometric standard stars and the SDSS stars in MD09 and magnitudes calculated from SED and SDSS magnitudes transformed to the Pan-STARRS1 system.

---

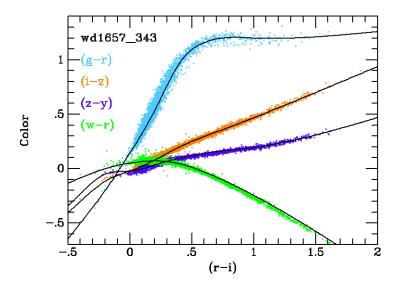[13]http://www.astro.washington.edu/users/ivezic/sdss/catalogs

Fig. 3.— The stellar locus calculated from SED integration is plotted over the locus of the stars near WD1657-343. This field has the lowest Galactic extinction of the standards, and has the longest integration time. The stellar magnitudes were averaged from all the observations.

Table 2: Pan-STARRS1 Photometric Consistency Checks.

| Filter | Std | ± | SDSS | ± | N |
|---|---|---|---|---|---|
| $g_{P1}$ | −0.004 | 0.007 | 0.014 | 0.012 | 2644 |
| $r_{P1}$ | −0.005 | 0.006 | −0.019 | 0.010 | 3072 |
| $i_{P1}$ | 0.008 | 0.009 | 0.008 | 0.011 | 2850 |
| $z_{P1}$ | −0.009 | 0.007 | 0.015 | 0.011 | 2816 |
| $y_{P1}$ | 0.005 | 0.010 | 0.001 | 0.013 | 2150 |
| $w_{P1}$ | 0.002 | 0.011 | — | — | — |

Note. — The columns are the filter, average difference for the standard stars between observed instrumental magnitude (flux) and that predicted from SED, scatter among the $\sim 24$ observations, average difference between Pan-STARRS1 magnitude and SDSS magnitude, RMS scatter, and number of stars compared. The SDSS comparison is restricted to stars in a 3 magnitude range: $15 < g < 18$ to $13 < y < 16$.

## 3.   THE Pan-STARRS1 PHOTOMETRIC SYSTEM

After iteration to determine the best fit parameters, we present Figure 4 showing the net Pan-STARRS1 collecting area as a function of wavelength for the six filters, i.e. $A(\nu)$. This is the product of the MODTRAN atmosphere at 1.2 airmass from elevation 3 km with 0.65 mm of PWV at sea level and 0.7 aerosol, the vignetted collecting area, the throughput function of Figure 1, and the filter transmissions.
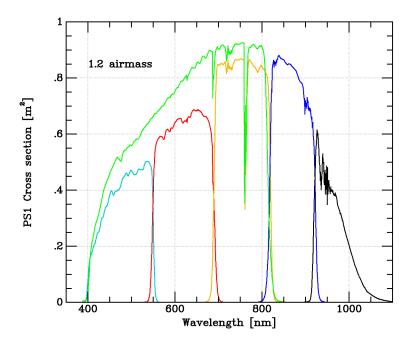


Fig. 4.— The Pan-STARRS1 capture cross section $A(\nu)$ in m²-e⁻/photon to produce a detected $e^-$ for an incident photon for the six Pan-STARRS1 bandpasses. This is at the standard airmass of 1.2, with standard PWV of 0.65 cm and aerosol exponent 0.7. Summary properties of each bandpass are found in Table 4.

A detailed spectral tabulation of the Pan-STARRS1 bandpasses is found in Table 3. Summary parameters of the Pan-STARRS1 bandpasses are found in Table 4. The "zero-points" are the AB magnitude of a neutral color (constant $f_\nu$) star that would produce 1 e⁻/sec in the detector with 1.2 airmasses of extinction. We also list the net atmospheric extinction *at 1.2 airmasses* we expect to see for an SED of constant $f_\nu$, so the sum of these two numbers is the "top of atmosphere" zeropoint for the Pan-STARRS1 system. We list these separately to emphasize that, however important it may be, extrapolation to "top of atmosphere" depends on SED of source and there is no unique correct answer, and also that

Table 3: Pan-STARRS1 Bandpasses

| $\lambda$ | $Open$ | $g_{\rm P1}$ | $r_{\rm P1}$ | $i_{\rm P1}$ | $z_{\rm P1}$ | $y_{\rm P1}$ | $w_{\rm P1}$ | Aero | Ray | Mol |
|---|---|---|---|---|---|---|---|---|---|---|
| ... | ... | ... | ... | ... | ... | ... | ... | ... | ... | ... |
| 550 | 0.675 | 0.323 | 0.367 | 0.000 | 0.000 | 0.000 | 0.662 | 0.962 | 0.924 | 0.971 |
| 551 | 0.678 | 0.248 | 0.423 | 0.000 | 0.000 | 0.000 | 0.665 | 0.962 | 0.924 | 0.971 |
| 552 | 0.682 | 0.175 | 0.469 | 0.000 | 0.000 | 0.000 | 0.668 | 0.962 | 0.925 | 0.971 |
| 553 | 0.685 | 0.113 | 0.504 | 0.000 | 0.000 | 0.000 | 0.670 | 0.962 | 0.925 | 0.971 |
| 554 | 0.688 | 0.068 | 0.528 | 0.000 | 0.000 | 0.000 | 0.672 | 0.963 | 0.926 | 0.970 |
| 555 | 0.689 | 0.041 | 0.544 | 0.000 | 0.000 | 0.000 | 0.673 | 0.963 | 0.927 | 0.970 |
| 556 | 0.690 | 0.025 | 0.556 | 0.000 | 0.000 | 0.000 | 0.674 | 0.963 | 0.927 | 0.969 |
| 557 | 0.691 | 0.015 | 0.565 | 0.000 | 0.000 | 0.000 | 0.674 | 0.963 | 0.928 | 0.968 |
| 558 | 0.691 | 0.009 | 0.570 | 0.000 | 0.000 | 0.000 | 0.675 | 0.963 | 0.928 | 0.968 |
| 559 | 0.693 | 0.006 | 0.575 | 0.000 | 0.000 | 0.000 | 0.678 | 0.963 | 0.929 | 0.967 |
| 560 | 0.695 | 0.003 | 0.578 | 0.000 | 0.000 | 0.000 | 0.680 | 0.963 | 0.929 | 0.966 |
| ... | ... | ... | ... | ... | ... | ... | ... | ... | ... | ... |

Note. — The columns are wavelength [nm] and capture cross-section [$m^2$-$e^-$/photon] for each of the Pan-STARRS1 bandpasses, *including* the nominal 1.2 airmasses of atmospheric extinction. The last three columns list the transmission of the Pan-STARRS1 standard atmosphere from aerosol scattering, Rayleigh scattering, and molecular absorption. Table 3 is published in its entirety in the electronic edition of the Astrophysical Journal. A portion is shown here for guidance regarding its form and content.

extinction is not linear in airmass. Equation 5 can be used to explore these dependencies. The sky brightnesses are AB mag per square arcsec, calculated for a dark sky model and observed between 2010-11-12 and 2011-05-12. Most of the discrepancy between calculated and observed comes from the degree to which moonlight impinges on normal operations, although the $y_{P1}$ brightness has recently been reduced by introduction of a new baffle.

Table 4: Pan-STARRS1 Bandpass Parameters

| Filter | $\langle A \rangle$ | $\lambda_{eff}$ | $\lambda_B$ | $\lambda_R$ | ZP | Extinct | $\mu$ | $\mu_{obs}$ |
|--------|------|------|------|------|------|------|------|------|
| $g_{P1}$ | 0.1212 | 481 | 414 | 551 | 24.56 | 0.22 | 22.12 | 21.92 |
| $r_{P1}$ | 0.1463 | 617 | 550 | 689 | 24.76 | 0.13 | 20.97 | 20.83 |
| $i_{P1}$ | 0.1435 | 752 | 690 | 819 | 24.74 | 0.09 | 20.18 | 19.79 |
| $z_{P1}$ | 0.0980 | 866 | 818 | 922 | 24.33 | 0.05 | 19.27 | 19.24 |
| $y_{P1}$ | 0.0393 | 962 | 918 | 1001 | 23.33 | 0.13 | 18.43 | 18.24 |
| $w_{P1}$ | 0.4739 | 608 | 433 | 815 | 26.04 | 0.15 | 20.86 | 20.62 |
| $Open$ | 0.6463 | 655 | 431 | 971 | 26.37 | 0.14 | 20.12 | 20.00 |

Note. — The columns are the filter, "net cross section" [m$^2$] for $f_\nu$=const through this filter at 1.2 airmasses ($\int A(\nu)d\ln\nu$), filter "pivot" wavelength [nm] described by Bessell & Murphy (2012) ($\int \lambda A(\nu)d\ln\nu/\langle A\rangle$), bandpass blue and red wavelengths [nm] obtained from a least-squares fit of a square bandpass, zeropoint at 1.2 airmasses [AB mag], extinction at 1.2 airmasses [mag] (*not* extinction per airmass!), calculated dark sky brightness [mag/$''$], and median observed sky brightness [mag/$''$].

## 3.1.  The Pan-STARRS1 Stellar Locus

The derivation of the synthetic Pan-STARRS1 stellar locus from the library of SEDs mentioned above first required removal of Galactic reddening. We started by undoing the correction applied by Gunn & Stryker (1983) for Galactic extinction, returning them to "as-observed" SEDs, although we kept their estimates of $A_V$. We then estimated a $V$ band extinction value for the rest of the stars by using the Parenago (1940) model recommended by Groenewegen (2008) (scale height of 90 pc and visual extinction of 1.08 mag/kpc), and using parallaxes from SIMBAD[14]. Uncertainties in parallax were folded into flux and color

[14]http://http://simbad.u-strasbg.fr/simbad/

uncertainties. Given a value for $A_V$ and adopting $R_V = 3.1$, we used the extinction curves from Fitzpatrick (1999) to calculate stellar SEDs with no reddening from dust, and then integrated magnitudes in all bandpasses

Table 5 lists spline knots fitted to this locus, using $(r-i)$ as the independent variable. The synthetic Pan-STARRS1 colors are seen in Figure 3. The prominent wiggle visible in the $(z-y)$ locus at $(r-i) \sim 0$, also visible in $(i-z)$, arises from Paschen absorption that peaks at spectral type A.

Table 5: Pan-STARRS1 Synthetic Stellar Locus

| $(r-i)$ | $(g-r)$ | $(i-z)$ | $(z-y)$ | $(z-J)$ | $(z-H)$ | $(y-J)$ | $(w-r)$ | $(O-r)$ |
|---|---|---|---|---|---|---|---|---|
| $-0.4$ | $-0.50$ | $-0.290$ | $-0.210$ | $0.12$ | $0.05$ | $0.34$ | $-0.085$ | $0.015$ |
| $-0.2$ | $-0.19$ | $-0.110$ | $-0.050$ | $0.48$ | $0.50$ | $0.50$ | $0.000$ | $0.070$ |
| $0.0$ | $0.15$ | $-0.030$ | $-0.025$ | $0.70$ | $0.87$ | $0.70$ | $0.050$ | $0.060$ |
| $0.2$ | $0.55$ | $0.090$ | $0.035$ | $0.89$ | $1.28$ | $0.86$ | $0.070$ | $-0.010$ |
| $0.4$ | $0.97$ | $0.200$ | $0.095$ | $1.14$ | $1.82$ | $1.00$ | $0.045$ | $-0.120$ |
| $0.6$ | $1.16$ | $0.295$ | $0.140$ | $1.22$ | $1.96$ | $1.11$ | $-0.030$ | $-0.280$ |
| $1.0$ | $1.20$ | $0.470$ | $0.195$ | $1.31$ | $2.00$ | $1.10$ | $-0.245$ | $-0.670$ |
| $2.0$ | $1.26$ | $0.940$ | $0.470$ | $1.23$ | $2.12$ | $0.87$ | $-0.940$ | $-1.820$ |

Note. — The columns provide knots for a natural spline for various Pan-STARRS1 and Pan-STARRS1-2MASS colors as a function of $(r-i)_{\mathrm{P1}}$.

The residuals of the synthetic colors from the 783 SEDs relative to the spline fits in Figure 5 demonstrate that the splines have accurately captured the variation.

## 3.2. Stellar Color Transformations

We used the synthetic magnitudes from the SEDs to fit for conversions between the Pan-STARRS1 photometric system and SDSS, Johnson/Cousins (Vega), and 2MASS (Vega). Both linear and quadratic versions are provided, with coefficients

$$y = A_0 + A_1 x + A_2 x^2 = B_0 + B_1 x. \qquad (6)$$

Figures 6 and 7 illustrate these relationships, and Table 6 provides the coefficients. We stress that these are computed for stellar SEDs and use for other SEDs may be less accurate. The
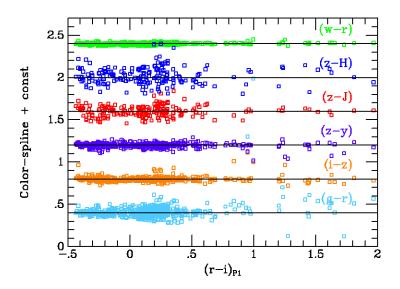
Fig. 5.— The residual of the Pan-STARRS1 colors we calculate for the SEDs relative to the spline fits. The RMS of the residual scatter is 0.09, 0.03, 0.03, 0.01, 0.06, 0.10 mag for $(g-r)$, $(i-z)$, $(z-y)$, $(w-r)$, $(z-J)$, and $(z-H)$.

marked deviations of $y_{\mathrm{P1}}$ and $z_{\mathrm{P1}}$ relative to $z_{SDSS}$ arise because of Paschen absorption and will differ for blue objects that lack hydrogen lines. The figures provide guidance about the validity of the linear or quadratic fits.
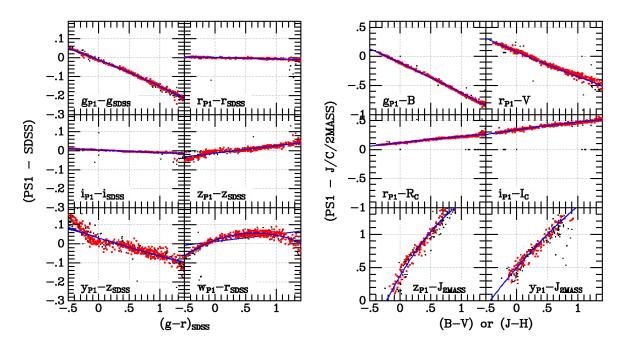


Fig. 6.— Comparison between the Pan-STARRS1 and SDSS bandpasses as a function of SDSS color (left) and Johnson, Cousins, and 2MASS bandpasses as a function $(B-V)$ or $(J-H)$ (right).

## 3.3. Pan-STARRS1 Galactic Extinction

Equipped with the Pan-STARRS1 bandpasses, we calculate the effects of Galactic extinction by applying 0.1 mag of $E(B-V)$ Galactic extinction to each of the SEDs and fitting the dimming in each of the Pan-STARRS1 bandpasses as a function of unreddened, Pan-STARRS1 stellar color. The extinction curve is from Fitzpatrick (1999) using $R_V = 3.1$, and the fits are valid for $-1 < (g - i) < 4$. These curves are illustrated in Figure 8.

Table 6: Pan-STARRS1 Bandpass Transformations

| $x$ | $y$ | $A_0$ | $A_1$ | $A_2$ | $\pm$ | $B_0$ | $B_1$ | $\pm$ |
|---|---|---|---|---|---|---|---|---|
| $(g-r)_{SDSS}$ | $(g_{P1}-g_{SDSS})$ | $-0.011$ | $-0.125$ | $-0.015$ | $0.006$ | $-0.012$ | $-0.139$ | $0.007$ |
| $(g-r)_{SDSS}$ | $(r_{P1}-r_{SDSS})$ | $0.001$ | $-0.006$ | $-0.002$ | $0.002$ | $0.000$ | $-0.007$ | $0.002$ |
| $(g-r)_{SDSS}$ | $(i_{P1}-i_{SDSS})$ | $0.004$ | $-0.014$ | $0.001$ | $0.003$ | $0.004$ | $-0.014$ | $0.003$ |
| $(g-r)_{SDSS}$ | $(z_{P1}-z_{SDSS})$ | $-0.013$ | $0.040$ | $-0.001$ | $0.009$ | $-0.013$ | $0.039$ | $0.009$ |
| $(g-r)_{SDSS}$ | $(y_{P1}-z_{SDSS})$ | $0.031$ | $-0.106$ | $0.011$ | $0.023$ | $0.031$ | $-0.095$ | $0.024$ |
| $(g-r)_{SDSS}$ | $(w_{P1}-r_{SDSS})$ | $0.018$ | $0.118$ | $-0.091$ | $0.012$ | $0.012$ | $0.039$ | $0.025$ |
| $(B-V)$ | $(g_{P1}-B)$ | $-0.108$ | $-0.485$ | $-0.032$ | $0.011$ | $-0.104$ | $-0.523$ | $0.013$ |
| $(B-V)$ | $(r_{P1}-V)$ | $0.082$ | $-0.462$ | $0.041$ | $0.025$ | $0.077$ | $-0.415$ | $0.025$ |
| $(B-V)$ | $(r_{P1}-R_C)$ | $0.117$ | $0.128$ | $-0.019$ | $0.008$ | $0.119$ | $0.107$ | $0.009$ |
| $(B-V)$ | $(i_{P1}-I_C)$ | $0.341$ | $0.154$ | $-0.025$ | $0.012$ | $0.343$ | $0.126$ | $0.013$ |
| $(J_{2MASS}-H_{2MASS})$ | $(z_{P1}-J_{2MASS})$ | $0.418$ | $1.594$ | $-0.603$ | $0.068$ | $0.428$ | $1.260$ | $0.073$ |
| $(J_{2MASS}-H_{2MASS})$ | $(y_{P1}-J_{2MASS})$ | $0.528$ | $0.962$ | $-0.069$ | $0.061$ | $0.531$ | $0.916$ | $0.061$ |
| $(g-r)_{P1}$ | $(g_{SDSS}-g_{P1})$ | $0.013$ | $0.145$ | $0.019$ | $0.008$ | $0.014$ | $0.162$ | $0.009$ |
| $(g-r)_{P1}$ | $(r_{SDSS}-r_{P1})$ | $-0.001$ | $0.004$ | $0.007$ | $0.004$ | $-0.001$ | $0.011$ | $0.004$ |
| $(g-r)_{P1}$ | $(i_{SDSS}-i_{P1})$ | $-0.005$ | $0.011$ | $0.010$ | $0.004$ | $-0.004$ | $0.020$ | $0.005$ |
| $(g-r)_{P1}$ | $(z_{SDSS}-z_{P1})$ | $0.013$ | $-0.039$ | $-0.012$ | $0.010$ | $0.013$ | $-0.050$ | $0.010$ |
| $(g-r)_{P1}$ | $(z_{SDSS}-y_{P1})$ | $-0.031$ | $0.111$ | $0.004$ | $0.024$ | $-0.031$ | $0.115$ | $0.024$ |
| $(g-r)_{P1}$ | $(r_{SDSS}-w_{P1})$ | $-0.024$ | $-0.149$ | $0.155$ | $0.018$ | $-0.016$ | $-0.029$ | $0.031$ |
| $(g-r)_{P1}$ | $(B-g_{P1})$ | $0.212$ | $0.556$ | $0.034$ | $0.032$ | $0.213$ | $0.587$ | $0.034$ |
| $(g-r)_{P1}$ | $(V-r_{P1})$ | $0.005$ | $0.462$ | $0.013$ | $0.012$ | $0.006$ | $0.474$ | $0.012$ |
| $(g-r)_{P1}$ | $(R_C-r_{P1})$ | $-0.137$ | $-0.108$ | $-0.029$ | $0.015$ | $-0.138$ | $-0.131$ | $0.015$ |
| $(g-r)_{P1}$ | $(I_C-i_{P1})$ | $-0.366$ | $-0.136$ | $-0.018$ | $0.017$ | $-0.367$ | $-0.149$ | $0.016$ |
| $(g-r)_{P1}$ | $(V-w_{P1})$ | $-0.021$ | $0.299$ | $0.187$ | $0.025$ | $-0.011$ | $0.439$ | $0.035$ |
| $(g-r)_{P1}$ | $(V-g_{P1})$ | $0.005$ | $-0.536$ | $0.011$ | $0.012$ | $0.006$ | $-0.525$ | $0.012$ |

Note. — The table provides the coefficients for Equation 6.
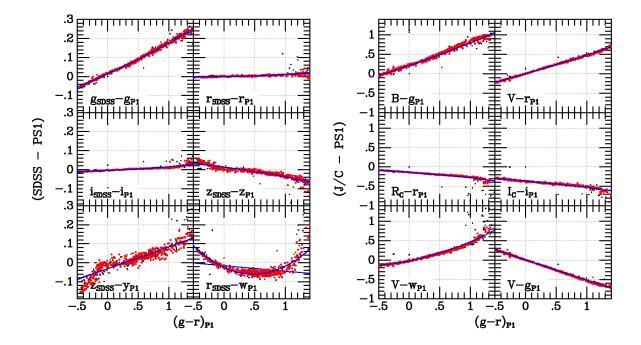
Fig. 7.— Comparison between the SDSS and Pan-STARRS1 bandpasses as a function of $(g-r)_{P1}$ (left) and Johnson and Cousins versus Pan-STARRS1 as a function $(g-r)_{P1}$ (right).

$((g-i) \sim 0.2 + 2.9(r-i)$ for $(r-i) < 0.5$.)

$$Ag/E(B-V) = 3.613 - 0.0972(g-i) + 0.0100(g-i)^2 \tag{7}$$
$$Ar/E(B-V) = 2.585 - 0.0315(g-i) \tag{8}$$
$$Ai/E(B-V) = 1.908 - 0.0152(g-i) \tag{9}$$
$$Az/E(B-V) = 1.499 - 0.0023(g-i) \tag{10}$$
$$Ay/E(B-V) = 1.251 - 0.0027(g-i) \tag{11}$$
$$Aw/E(B-V) = 2.672 - 0.2741(g-i) + 0.0247(g-i)^2 \tag{12}$$
$$Ao/E(B-V) = 2.436 - 0.3816(g-i) + 0.0441(g-i)^2 \tag{13}$$

Note that Schlafly & Finkbeiner (2011) recommend a recalibration of the $E(B-V)$ from Schlegel et al. (1998) which amounts to multiplication by 0.88. Therefore when the formulae above are multiplied by $E(B-V)$ in order to obtain a Pan-STARRS1 extinction, they should also be multiplied by an additional factor of 0.88 if $E(B-V)$ is derived from SFD.
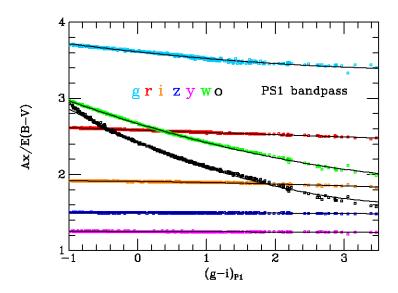
Fig. 8.— Computed galactic extinction coefficient, $A_x/E(B-V)$ in the Pan-STARRS1 bandpasses as a function of stellar color. (Note that $E(B-V)$ from the SFD catalog should be multiplied by 0.88.)

## 3.4. Filter and Detector Color Terms

The Pan-STARRS1 filter's response varies as a function of field angle, although we believe them to be quite uniform as a function of azimuth. As a function of angle off of the boresight we list color terms for stellar SEDs in Table 7, meaning the slope of the response in each filter as a function of $(r-i)$. (This creates offsets in response to SEDs of different color than the color of the flatfields, which is approximately that of a K star.) The units are magnitude per unit $(r-i)$ with the usual sign: negative implies more sensitivity for redder SEDs. The $g_{P1}$ filter in particular is more red sensitive at large field angle because the red edge of the bandpass shifts to the red by almost 10 nm. These offsets do not change for SEDs redder than $(r-i) = 0.5$.

Table 7: Pan-STARRS1 Filter Color Terms

| $\theta$ | $g' - g$ | $r' - r$ | $i' - i$ | $z' - z$ | $y' - y$ | $w' - w$ |
|------|---------|---------|---------|---------|---------|---------|
| 0.00 | −0.008 | −0.005 | −0.006 | −0.005 | −0.011 | −0.009 |
| 0.15 | −0.006 | −0.003 | −0.006 | −0.005 | −0.011 | −0.009 |
| 0.30 | 0.002 | −0.000 | −0.002 | −0.003 | −0.010 | −0.008 |
| 0.45 | 0.002 | 0.002 | −0.003 | −0.002 | −0.008 | −0.007 |
| 0.60 | 0.002 | 0.003 | −0.004 | −0.003 | −0.006 | −0.004 |
| 0.75 | 0.003 | 0.004 | −0.001 | −0.002 | −0.004 | 0.002 |
| 0.90 | 0.002 | 0.004 | 0.001 | −0.000 | −0.001 | 0.005 |
| 1.05 | −0.003 | 0.002 | −0.000 | −0.001 | 0.001 | 0.006 |
| 1.20 | −0.006 | 0.000 | 0.002 | −0.001 | 0.003 | 0.008 |
| 1.35 | −0.010 | 0.001 | 0.005 | 0.002 | 0.005 | 0.008 |
| 1.50 | −0.020 | −0.002 | 0.007 | 0.006 | 0.005 | 0.005 |
| 1.65 | −0.033 | −0.007 | 0.009 | 0.010 | 0.004 | 0.005 |

Note. — The table provides color terms [mag/mag$(r-i)$] for each filter as a function of field angle [deg]. These offsets do not change for SEDs redder than $(r-i) = 0.5$.

The bandpass shapes have negligible sensitivity to CCD temperature except in the $y_{P1}$ band, where the CCDs become more sensitive by $-0.0004$ mag/K/$(r-i)$. Note that this is the *differential* sensitivity as a function of color — the overall sensitivity increase is about an order of magnitude greater, $\sim -0.003$ mag/K.

There is some variation in QE between OTAs, but the color sensitivity is small in $r_{P1}$, $i_{P1}$,

$z_{P1}$, and $y_{P1}$(less than 0.01mag/mag). Variations in the AR coatings do create sensitivity changes in $g_{P1}$ and $w_{P1}$, however. Table 8 lists the $g_{P1}$ color terms for each OTA. To be explicit, OTA 34 has a color term of +0.020, meaning that it has 1% greater response than the mean of all OTAs for an SED of $(r-i) = 0$ than it does for $(r-i) = 0.5$.

Table 8: Pan-STARRS1 OTA Color Terms for $g_{P1}$

| OTA77 | −0.018 | −0.007 | −0.001 | −0.042 | −0.012 | −0.012 | OTA70 |
|---|---|---|---|---|---|---|---|
| −0.045 | 0.015 | −0.007 | −0.002 | 0.017 | −0.003 | −0.016 | −0.049 |
| −0.012 | −0.001 | 0.007 | 0.008 | −0.012 | 0.005 | 0.037 | −0.005 |
| −0.016 | 0.003 | 0.007 | −0.022 | 0.020 | 0.038 | 0.003 | −0.017 |
| 0.001 | −0.012 | −0.002 | −0.025 | 0.003 | 0.001 | 0.006 | −0.004 |
| −0.008 | −0.003 | 0.000 | 0.010 | −0.019 | −0.032 | 0.010 | 0.005 |
| −0.015 | −0.018 | −0.040 | −0.012 | 0.002 | −0.003 | −0.034 | −0.013 |
| OTA07 | −0.010 | −0.019 | −0.007 | 0.029 | −0.007 | −0.012 | OTA00 |

Note. — The table provides $g_{P1}$ color terms [mag/mag$(r-i)$] for each OTA according to its conventional position in GPC1. These offsets do not change for SEDs redder than $(r-i) = 0.5$.

## 4.   SYSTEMATIC ERRORS

With more than a hundred high signal-to-noise observations of spectrophotometric standards and comparisons of thousands of stars with existing catalogs, the statistical error of this determination of the Pan-STARRS1 photometric system is tiny. In this section we describe our best estimates of the remaining systematic error, derived both from the uncertainties in the contributing calculations as well as whatever external tests we can perform.

The comparison between in-situ measurement of filter transmission and that performed by Barr only probed one radius, and the match was excellent but not exact. We have attempted to compensate for any spectral tilt and mean, but we estimate that with 90% confidence the filter edges are not off by more than 1 nm and the transmission tilt is not more than ±1% across any bandpass. (For example $r_{P1}$ is perhaps slightly more blue sensitive than the Barr curves and $w_{P1}$ slightly more sensitive in the middle of the band.) Integrating these limits against power law SEDs yields 3–5 millimag of offset per unit $(r-i)$ from error in band edge and 1–3 millimag from spectral tilt ($z_{P1}$ to $g_{P1}$). We therefore estimate the

systematic uncertainty in photometry from imperfect knowledge of filters at 90% confidence to be comparable to but smaller than the filter color terms listed in Table 7.

Similarly, the "tweak" function corrects the laser-derived throughput, imposing tilts as large as $\pm 3\%$ in $g_{P1}$, and therefore correcting a color term as large as 10 millimag per unit $(r-i)$ relative to Calspec colors. We do not have any external corroboration of the accuracy of this correction, but we estimate that it is accurate enough to bring its contributions to systematic error down to the same level as that which might be present in the filter curves, 1–3 millimag.

Use of MODTRAN does not alter the fact that we are fundamentally extrapolating observations of spectrophotometric standards between airmass 1–2 to other airmass. In each filter we find an RMS of $\sim 0.01$ mag among $\sim 20$ observations of 7 stars distributed more or less uniformly between airmass 1.0–1.7. Formally, the uncertainty in extrapolating to airmass 0 is somewhere around 0.02–0.03 mag, regardless of whether the extinction was $\sim 0.18$ mag per airmass for $g_{P1}$ or $\sim 0.04$ mag per airmass for $z_{P1}$. The legacy of that exercise was not a system zeropoint to be applied on different nights, however, but rather "top of atmosphere" $grizyw$ magnitudes for $3 \times 10^5$ stars. These magnitudes are differential measurements to Calspec spectrophotometric standards taken at the same airmass, and therefore their formal error is of order 3 millimag, regardless of filter. In fact clouds and aerosols can be patchy and do vary on short timescales, but we believe that the scatter in the standard observations puts a bound on how large that effect can be. We therefore estimate with 90% confidence that the systematic error arising from atmospheric extinction is no greater than 5 millimag.

It is well known that the PSF is complex and carries considerable flux to large angle. It is typically modeled as a core from atmospheric, guiding, and optics blurring, followed by a $\theta^{-3}$ skirt from diffraction, finally succeeded by a $\theta^{-2}$ skirt from small particle scattering. This last component generally does not dominate until larger angle than is used as a "reference aperture", but some 5–10% of the net flux is scattered beyond any reasonable aperture, and its loss is normally accounted as a loss in throughput (dust and degradation) and miniscule enhancement in sky level. Differential assessment of the fluxes of stars relative to standards via a single photometry algorithm and reference aperture sidesteps these PSF issues provided the PSF model does not have biases as a function of magnitude or PSF shape, except for two purposes. The first case arises when comparing stellar photometry to surface brightnesses of large galaxies, as noted by Tonry *et al.* (1997). The second case arises if we ever try to do absolute photometry and our reference has different scattering properties than our unknown (perhaps because it has a different SED or the quantity of dust has changed). This change is only visible in PSFs, and a throughput evaluated using a flatfield or massively defocussed bright star will not detect it. It is not inconceivable that the "tweak" required to

bring standard star fluxes into agreement with Calspec standards has to do with chromatic differences in the large angle scattering and systematic differences in the PSF of blue versus red objects, but it is beyond the scope of this work to delve deeper into this possibility.

For this exercise we have used a single photometry algorithm, IPP's PSPhot, restricted to relatively bright objects. We note that differences between the flux found by PSPhot, DoPhot, Sextractor, and other photometry algorithms do exist at the 0.02 mag level, and they do seem to be related to the "winginess" of the PSF. Also, errors do enter from the procedure of constructing an aperture magnitude from a PSF fit magnitude and/or application of a curve of growth to a fixed metric aperture. We believe that systematic errors of at least 10 millimag will arise depending on optics cleanliness and PSF changes, but most will be taken out by a nightly regression of flux as a function of airmass. We believe that the systematic errors incurred in comparing the PSPhot flux of relatively bright spectrophotometric standards to others on this particular night is not larger than 5 millimag.

Our photometric system is based on both direct comparison with the 7 Calspec stars as well as comparing the stellar locus found in the 7 Calspec star fields and MD09 with the stellar locus of all 783 SEDs, and the agreement provides some level of check on systematic error. The stellar locus comparison depends on removal of dust reddening, whose uncertainty we calculated as best we could. It also depends on the consistency and homogeneity of the SEDs, but we could not detect significant differences between the various sources. By adjustment of the tweak function we were able to simultaneously match the results from the 7 Calspec stars to 6 millimag RMS and the cross-filter stellar locus of three fields, MD09, WD1657, and LDS749b to 10 millimag RMS. We regard this as confirmation of our 90% confidence that our net systematic difference from the 7 Calspec standards is 10 millimag or less.

Although we did not measure absolute fluxes from the laser experiments nor independently measure the pupil of the telescope, by knowing the individual throughputs of the optical components and theoretical ray traces we have created a crude absolute photometer. If we had included a contribution for dust or wide angle scattering it is plausible that we would have decided on a mean loss of 8% relative to clean optics. Although the non-constancy of the tweak function required to match SEDs was disappointing, it does confirm that these SEDs are accurately on the AB system within several percent.

The question of how accurately the SEDs conform to the AB system is complex. Bohlin (2007) describes how the Calspec system is founded on NLTE models of hot, hydrogen white dwarfs and an absolute flux for Vega. We find good consistency among the 7 Calspec stars, although the fluxes we observe for 1740346 and possibly P177D are lower by approximately 0.02 mag in $i_{P1}$ and $w_{P1}$ relative to Calspec than WD1657 and the three KF stars. Although our knowledge of $i_{P1}$ and $w_{P1}$ may flawed, we also note that there is a discontinuity at 800 nm

where the STIS spectra give way to NICMOS in the Calspec SEDs for WD1657 and the KF stars, but not for 1740346 and P177D. Our photometry may indicate a small discrepancy in some of the Calspec SEDs, but of course we do not know which is correct.

A more direct comparison of SEDs is also revealing. Fukugita et al. (1996) list SEDs for Vega and BD+17 4708. Integrating the SDSS bandpasses against these and the Calspec SEDs yields $(g-z)$ colors that are 24 millimag redder for the SDSS SEDs than the Calspec SEDs. The NGSL SED for BD+17 4708 differs very substantially from that of Calspec, with a difference in $(g-z)$ of 87 millimag. (Although the NGSL data for BD+17 4708 was subject to a slit mis-center of 0.84 pixels, that is less than the 0.90 pixel limit for which the web page cautions about the quality of the V2 correction.)

We have no way to know which of these SEDs is in error, although we do favor the Calspec set because of use of HST, the care with which each star has been checked, and magnitudes that are usefully faint. We also believe that the use of white dwarf models (H and He) will prove to be superior to subdwarf stars and Vega. BD+17 4708 is too bright for Pan-STARRS1 so we cannot offer support for Calspec versus NGSL, but we do encourage the community to note and resolve these differences!

Our 90% confidence estimate for the absolute AB accuracy of the Calspec set of SEDs is 20 millimag. We do not believe that it is presently possible to compare a $g$ magnitude at redshift 0 to a $z$ magnitude at redshift 1 without incurring this level of photometric uncertainty.

When we compare the Pan-STARRS1 magnitudes of stars in the MD09 field with those tabulated by SDSS as part of Stripe82, we find statistically significant offsets listed in Table 2. In particular $g_{SDSS} - g_{P1}$ is bright by 14 millimag and $r_{SDSS} - r_{P1}$ is faint by 19 millimag, causing the SDSS $(g-r)$ color to be bluer for a given star than that of Pan-STARRS1 by 33 millimag. We believe that this may partially arise because of the difference in the SDSS and Calspec SEDs: if the SDSS standards are redder than Calspec the derived magnitudes will be bluer. Doi et al. (2010) has described the evolution of the SDSS bandpasses over time, and enough change has occurred to create this level of discrepancy if the SDSS bandpasses we have adopted from the web page are not correct, since that is how we transform SDSS magnitudes onto the Pan-STARRS1 system for comparison. It is also possible that the cataloged magnitudes are somewhat heterogeneous and have acquired offsets from the AB system because of filter evolution.

Fukugita et al. (2011) have performed a detailed comparison of SDSS catalog magnitudes with synthetic magnitudes and find an offset $\Delta(g-r)_{spec-photo} = 0.026(g-r) + 0.008$, or +21 millimag in the sense of cataloged magnitudes being bluer than synthetic magnitudes when

evaluated at a common stellar color of $(g-r) = 0.5$ (close to the discrepancy we see). We also agree with Fukugita et al. (2011) about the sign and magnitude of the discrepancy in $(r-i)$ (but note the missing minus in their equation for $\Delta(r-i)_{spec-photo}$), and these could both be alleviated by adjusting $r_{SDSS}$ brighter by about 30 millimag.) For Fukugita et al. (2011) "This implies that the response curves are well characterized," but we believe that Pan-STARRS1 and SDSS can do better.

As a final comparison we illustrate differences between SDSS DR7 (Abazajian et al. 2009), SDSS DR8 (Finkbeiner, private communication), and the Stripe82 compilation from Ivezic in Figure 9. The points from the three comparisons are just overlaid, and the lines illustrate the differences between the three SDSS calibrations. (We find that the relations are quite transitive, so these differences also appear when SDSS is intercompared directly.) We are therefore inclined to believe that Pan-STARRS1 is closer to the AB system than are
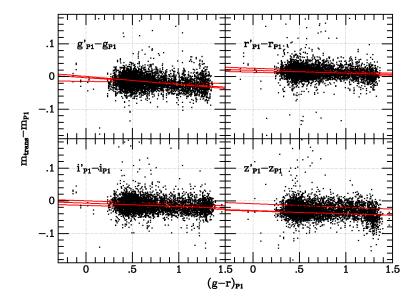


Fig. 9.— Comparison between stellar magnitudes in MD09 from three SDSS releases, transformed to the Pan-STARRS1 system, and the corresponding Pan-STARRS1 magnitudes. The Ivezic Stripe82 fits differ particularly for $g_{P1}$ (small trend with color, but offset from zero) and $z_{P1}$ (much closer to zero than DR7 and DR8).

the extant SDSS catalogs, but the matter deserves more detailed study.

We do not find Figure 9 at all discouraging because the offsets and slopes are small and very evident, given the quality of the photometry. We are confident that the "ubercal" procedure introduced by Padmanabhan et al. (2008) and presently being applied to the 3/4

sky surveyed by Pan-STARRS1 (Schlafly & Finkbeiner 2012) will succeed in creating an all-sky photometric system with systematic error below 10 millimag. Merging the SDSS stripes with the Pan-STARRS1 footprints will help reduce the errors of both and create a very homogeneous system.

We summarize our best estimates of 90% systematic uncertainties in Table 9. The most serious systematic uncertainty comes from the tie between SED and physical units.

Table 9: 90% Confidence Systematic Error Estimates [millimag]

| Source | Uncertainty | Notes |
|---|---|---|
| Filter edges | 3–5 | bigger for broader bandpasses |
| Filter transmission | 1–3 | bigger for broader bandpasses |
| Tweak determination | 3–5 | bigger at ends of spectrum |
| Atmospheric extinction | 3–5 | bigger for bluer wavelengths |
| Flux determination | 5–10 | inter-night worse |
| Net offset wrt Calspec | 10 | 7 std, single photometric night |
| SED conformity to AB | 20 | uncertain |

## 5. SUMMARY

We have described the Pan-STARRS1 system, comprising telescope, detector, and software. Arguing that the photometric properties can be factored into slowly varying terms (optics, filters, and detector) and rapid terms (atmosphere), we have endeavored to measure each and to provide a consistent set of bandpasses and a methodology for determining the atmospheric transmission.

All optical components and the detector QE were measured separately in the lab and we measured them in-situ with calibrated, monochromatic beams of light. We found good agreement; however, we found that approximately 8% of light is lost relative to lab measurements, presumably because of absorption or scattering by dust and dirt that have accumulated, and we suspect that one or more lens AR coatings do not match design.

We have used MODTRAN models to characterize atmospheric transmission. These are adjusted into agreement with the conditions on a given night by matching the observed regression against airmass for different filters to the aerosol content of the model. We also have deployed a telescope with full-aperture diffraction grating to monitor the spectrum of

Polaris and constrain the water content of the MODTRAN models from the equivalent width observed in water bands.

The combination of optics and filter transmission with atmospheric transmission gives us a net cross-section of the Pan-STARRS1 system to convert a photon arrival rate to a detected signal. For a source whose AB spectrum is known except for a normalization, we can thereby invert the observed signal and obtain an absolute AB magnitude.

The comparison with spectral energy distributions was carried out on a night of exceptional clarity devoted to observations of 7 Calspec spectrophotometric standards, observed with no filter and in all filters at a wide range of airmasses. This comparison revealed the need for an 0.03 mag RMS "tweak" correction to our in-situ measurements of throughput across the optical whose origin we do not understand. By tweaking the in-situ measurements into agreement with the spectrophotometric standards we obtained transmission functions for the optics and for each filter, and we have therefore made the Calspec standards the basis for the Pan-STARRS1 photometric system.

Given Pan-STARRS1 bandpasses, we provide a number of useful products, such as an unreddened stellar locus, Galactic extinction coefficients as a function of $E(B-V)$, and stellar color transformations between Pan-STARRS1 and other photometric systems. We also present the color terms in the Pan-STARRS1 system that appear as a function of field angle among the filters and between the 60 different CCDs.

We finished with a discussion of the (small) random errors and (more serious) systematic errors that remain in the Pan-STARRS1 system. We believe that we have tied the Pan-STARRS1 system to the 7 Calspec SEDs to the 10 millimag level or better, but we believe that it is possible that errors as large as 20 millimag may still exist between the Calspec SEDs and the AB system. Comparison with stars cataloged by SDSS reveal excellent agreement as well as systematic offsets at the $\sim 20$ millimag level that we have argued can be traced to systematic errors in the SDSS bandpasses and systematic differences between SDSS spectrophotometry and Calspec.

In the future we certainly will obtain observations of more spectrophotometric standards on photometric nights. There are $\sim 20$ Calspec stars faint enough not to saturate during ordinary observing that are particularly useful.

The "ubercal" product being generated by Schlafly & Finkbeiner (2012) may also reveal some interesting systematics while it is creating a homogeneous catalog of stars around the sky. In particular we look forward to the learning how the many epochs of "ubercal" magnitudes for the various Calspec standards match up, as well as the $\sim 50$ sq. deg. observed on MJD 55744. It would be worth integrating the SDSS spectrophotometric SEDs against

these Pan-STARRS1 bandpasses to obtain their Pan-STARRS1 magnitudes for comparison with the "ubercal" magnitudes.

The "tweak" difference between in-situ throughput measurements and spectrophotometry was disagreeably but not surprisingly large. It seems likely that the atmosphere is *not* a primary impediment to squeezing the accuracy of absolute photometry below the 1% level, and we could certainly do a much better job with our in-situ measurements, both relative and absolute. With some effort it should be possible to modify our ground-based measurements to the point that they provide useful constraints on white dwarf models and SEDs measured by HST. We look forward to the success of the ACCESS rocket experiments (Kaiser et al. 2010) that seek to improve the absolute calibration of Vega and BD+17 4708. It is certainly straightforward to design new, special purpose equipment to do absolute spectrophotometry from the ground, based on NIST calibration of photodiodes, that could reach the 1% level. Although we have no immediate plans to carry out such experiments, we emphasize that knowledge of absolute spectrophotometry is the main limitation in our current ability to do precision photometry, and we encourage the community to support efforts to improve it.

*Facilities:* PS1 (GPC1)

## REFERENCES

Abazajian, K. N., Adelman-McCarthy, J. K., Agüeros, M. A., et al. 2009, ApJS, 182, 543

Anderson, G. P., *et al.*, 2001 Proc. of the SPIE, **4381**, 455

Bessell, M. S. 1999, PASP, 102, 1181

Bessell, M. S. 2005, ARA&A, 43, 293

Bessell, M., & Murphy, S. 2012, PASP, 124, 140

Bohlin, Dickinson, & Calzetti, 2001, AJ, 122, 2118

Bohlin, R. C. 2007, The Future of Photometric, Spectrophotometric and Polarimetric Standardization, 364, 315

Burke, D. L., Axelrod, T., Blondin, S., et al. 2010, ApJ, 720, 811

Chambers, K. C, *et al.*, in preparation.

Cohen, M., Wheaton, W. A. & Megeath, S. T., 2003 AJ, 126, 1090

Covey, K. R., et al. 2007, AJ, 134, 2398

Doi, M. et al. 2010, AJ, 139, 1628

Fitzpatrick, E. L. 1999, PASP, 111, 63

Fukugita, M., Ichikawa, T., Gunn, J. E., et al. 1996, AJ, 111, 1748

Fukugita, M., Yasuda, N., Doi, M., Gunn, J. E., & York, D. G. 2011, AJ, 141, 47

Groenewegen, M. A. T. 2008, A&A, 488, 935

Gunn, J.E., & Stryker, L.L. 1983, ApJS, 52, 121

Gunn, J. E., Carr, M., Rockosi, C., et al. 1998, AJ, 116, 3040

Hayes, D. S., & Latham, D. W. 1975, ApJ, 197, 593

Hayes, D. S. 1985, Calibration of Fundamental Stellar Quantities, 111, 225

High, F. W., Stubbs, C. W., Rest, A., Stalder, B., & Challis, P. 2009, AJ, **138**, 110.

Hodapp, K. W., Siegmund, W. A., Kaiser, N., Chambers, K. C., Laux, U., Morgan, J., & Mannery, E. 2004, Proc. SPIE, **5489**, 667

Kaiser, M. E., Kruk, J. W., McCandliss, S. R., et al. 2010, Proc. SPIE, 7731,

Kaiser, N., et al. 2010, Proc. SPIE, 7733, 12K.

Magnier, E. 2006, Proceedings of The Advanced Maui Optical and Space Surveillance Technologies Conference, Ed.: S. Ryan, The Maui Economic Development Board, p.E5

Magnier, E., *et al.*, in preparation.

Oke, J. B., & Gunn, J. E. 1983, ApJ, 266, 713

Onaka, P., Tonry, J. L., Isani, S., Lee, A., Uyeshiro, R., Rae, C., Robertson, L., & Ching, G. 2008, Proc. SPIE, **7014**, 12.

Padmanabhan, N., Schlegel, D. J., Finkbeiner, D. P., et al. 2008, ApJ, 674, 1217

Parenago, P. P. 1940, Astron. Zh., 17, 3

Patat, F., Moehler, S., O'Brien, K., et al. 2011, A&A, 527, A91

Pickles, A.J. 1998 PASP, 110, 863

Schechter, P. L., Mateo, M., & Saha, A. 1993, PASP, 105, 1342

Schlafly, E. F., & Finkbeiner, D. P. 2011, ApJ, 737, 103

Schlafly, E. F., & Finkbeiner, D. P. 2012, in preparation

Schlegel, D. J., Finkbeiner, D. P., & Davis, M. 1998, ApJ, 500, 525

Shivvers, I. *et al.*, in preparation

Simons, D. A., & Tokunaga, A. 2002, PASP, 114, 169

Stubbs, C. W., & Tonry, J. L. 2006, ApJ, 646, 1436

Stubbs, C. W., High, F. W., George, M. R., et al. 2007, PASP, 119, 1163

Stubbs, C. W., Doherty, P., Cramer, C., Narayan, G., Brown, Y. J., Lykke, K. R., Woodward, J. T., & Tonry, J. L. 2010, ApJS, 191, 376

Tonry, J. L., Blakeslee, J. P., Ajhar, E. A., & Dressler, A. 1997, ApJ, 475, 399

Tonry, J. L., Burke, B. E., Isani, S., Onaka, P. M., & Cooper, M. J. 2008, Proc. SPIE, **7021**, 9.

York, D. G., et al. 2000, AJ, 120, 1579